# Catalysis Science & Technology

Accepted Manuscript






ROYAL SOCIETY OF CHEMISTRY

www.rsc.org/catalysis

Journal Name

ARTICLE

# Enhanced Activity of $H_2O_2$-treated Copper (II) Oxide Nanostructures for the Electrochemical Evolution of Oxygen

Received 00th January 20xx,
Accepted 00th January 20xx

DOI: 10.1039/x0xx00000x

www.rsc.org/

Albertus D. Handoko,[a,‡] Suzi Deng,[b,‡] Yilin Deng,[a,‡] Andy Wing Fai Cheng,[a] Kuang Wen Chan,[a] Hui Ru Tan,[c] Yanlin Pan,[a] Eng Soon Tok,[b] Chorng Haur Sow,[b] and Boon Siang Yeo[a,*]

The successful design and synthesis of earth-abundant and efficient catalysts for the oxygen evolution reaction (OER) will be a major step forward towards the use of electrochemical water splitting as an environmental-friendly process for producing $H_2$ fuel. Due to their poor activity, copper-based materials have not been considered apt for catalysing OER. In this work, we demonstrate that unique copper (II) oxide nanostructures obtained via hydrothermal synthesis and subsequent hydrogen peroxide treatment exhibit unusually high and sustainable OER activity. In 0.1 M KOH electrolyte, the CuO nanostructures catalyse OER with currents at 2.6-3.4 mA $cm^{-2}$ at 1.75 V (vs. RHE). The calculated turnover frequency (per Cu site) of ~$2\times10^{-3}$ $s^{-1}$ for $O_2$ production is markedly higher than that of high-surface area electrodeposited Cu metal nanoparticles by 40-68 times. The OER activity of the CuO nanostructures is also stable, approaching about half of 20% $IrO_x$/Vulcan XC-72 after an hour long OER. In-situ Raman spectroscopy at OER-relevant potentials recorded compelling evidence that $Cu^{III}$ active species may be responsible for the unusual OER activity of the CuO nanostructures, as indicated by its signature vibration at 603 $cm^{-1}$. This hitherto unobserved peak is assigned, with the aid of the model compound $NaCu^{III}O_2$, to the Cu-O stretching vibration of $Cu^{III}$ oxide. This feature was not found on electrodeposited Cu metal, which exhibited correspondingly weaker OER activity. The enhanced catalysis of $O_2$ evolution by the CuO nanostructures is thus attributed to not just its higher surface area, but also to the higher population of $Cu^{III}$ active sites on its surface.

## Introduction

The lack of cheap and efficient catalysts to reduce the significant overpotential required for the anodic oxygen evolution reaction (OER) is a major bottleneck in the realisation of water splitting as an environmental-friendly process to produce hydrogen gas fuel.[1] This critical step occurs in alkaline electrolytes via the reaction $4OH^- \rightarrow 2H_2O + 4e^- + O_2$. To date, the most efficacious electrocatalysts for water oxidation are the oxides of ruthenium[2] or iridium.[3] However, these metals are amongst the rarest and costliest elements on earth and hence, are not practical for industrial-scale applications. The OER activities of ruthenium[4] and iridium oxides[5] are also known to decrease over time in alkaline electrolytes. Promising OER activities have been observed using cobalt, manganese and nickel based compounds.[5] However, these metals have relatively high cost as they are used in the synthesis of magnetic materials.[6] The toxicity of manganese and nickel also requires extra care during synthesis and handling. For these reasons, there is an intensive ongoing effort to develop earth-abundant, cheap, safe and efficient electrocatalysts for oxygen evolution.

Copper is 60,000× more abundant and 3,000× cheaper than iridium.[7] It can also be facilely manipulated into various Cu and Cu oxide structures via hydrothermal synthesis[8] and electrodeposition.[9] This makes it easier to elucidate the fundamental composition-properties relationship of Cu catalysts and scale up their production for industry level usage. However, despite these advantages and its low toxicity,[10] copper or copper based compounds or complexes are rarely employed as OER catalysts. This is because copper metal, in itself, exhibits poor OER activity, that is on the same order as gold,[11] or approximately two orders of magnitude lower than $Co_3O_4$.[12] The dissolution of metallic copper in alkaline electrolytes[13-15] has also made it an inapt anode material in the water electrolyser. Copper oxides are perceived as unfavourable for electrocatalytic oxygen evolution reactions due to their lower conductivity.[16] However, more recent works have demonstrated that Cu-based catalysts, especially in their nanocrystalline form, can deliver promising OER

[a] Department of Chemistry, National University of Singapore, 3 Science Drive 3, Singapore 117543.
[b] Department of Physics, National University of Singapore, 2 Science Drive 3, Singapore 117542.
[c] Institute of Materials Research and Engineering, A*STAR (Agency for Science, Technology and Research), 3 Research Link, Singapore 117602.
‡ These authors contributed equally.
* Corresponding author. Email: chmyeos@nus.edu.sg

Electronic Supplementary Information (ESI) available: [(1) Detailed characterisation of catalysts described in this manuscript, (2) Online mass spectrometry data, (3) Calculation of turnover frequencies, (4) Surface area estimation, (5) stability assessments, (6) Details on Raman measurements and peak assignments, (7) Synthesis and characterisation of $Cu^{III}$-containing $NaCuO_2$]. See DOI: 10.1039/x0xx00000x

performances.[17-20] Among the reported Cu-based OER catalysts, only copper-rhodium delafossite ($CuRhO_2$) displays comparable OER performance to $Co_3O_4$.[19] Unfortunately, the high Rh content in this compound renders it economically unfeasible as a replacement for iridium.

Upon electrochemical oxidation, Cu metal has been reported to oxidize progressively to $Cu_2O$, $Cu(OH)_2$, CuO, and $Cu^{III}$ oxides.[21-25] Cyclic voltammograms (CV) of copper surfaces show an anodic peak at 1.5 V, prior to oxygen evolution, that has been assigned to the formation of $Cu^{III}$ oxides (all potentials cited in this work are with respect to the reversible hydrogen electrode, RHE).[23, 26] This finding suggests that highly oxidised Cu species could participate in the water oxidation, akin to the role of $Co^{IV}$ ions in the same reaction.[27, 28] The stronger resistance of Cu oxides towards corrosion in alkalis, as compared to Cu metal,[13, 29] is also likely to contribute to the stability of Cu-based catalysts during prolonged electrochemical oxygen evolution in water electrolysers.

In this work, we demonstrate that aggregates of CuO nanostructures obtained via hydrothermal synthesis and $H_2O_2$ treatment exhibit sustainable and excellent OER activity. The OER activity of these $H_2O_2$-treated CuO nanostructures is remarkably higher than that of electrodeposited Cu metal by 40-68 times. The OER current of the CuO nanostructures is also very stable as demonstrated by chronoamperometry. Very interestingly, in-situ Raman spectroscopy of the CuO nanostructures revealed the presence of a metastable surface species during OER. This species, which we assign to be $Cu^{III}$ oxide, is proposed to be the active sites for catalysing OER. Higher-valence $Cu^{III}$ species have been suspected to play a role in the electrochemical oxygen evolution reaction, although spectroscopic evidence of its presence has never been found.[23] The timely discovery of an OER active species on copper oxide surfaces is unprecedented, and a deeper understanding of its chemistry will inspire development of a new class of cheap, safe and earth-abundant OER catalysts.

## Result and Discussions

Nanostructured CuO powders were prepared by first synthesising $Cu_2O$ nanostructured precursors using the hydrothermal method, followed by $H_2O_2$ oxidation treatment (supporting information section 1.1 and 1.2.1). The as grown CuO nanostructures appear as 300-1000 nm elongated fragments, whose surfaces are densely decorated with ~5-10 nm CuO nanoparticles (Figure 1a-c). X-ray diffraction analysis confirmed the chemical identity of the sample as CuO with a volume-weighted crystallite size of 12.6 nm (Figure 1d, supporting information section 1.2.2.). This assignment is corroborated by Auger Cu LMM peak at a kinetic energy of 917.5 eV and Cu $2p_{3/2}$ peak at a binding energy of 934.1 eV (Figure 1e, supporting information section 1.3.).[30] The formation of CuO nanoparticles on the surface of the nanostructures was attributed to the highly oxidising properties of $H_2O_2$ that is capable of inducing growth of small

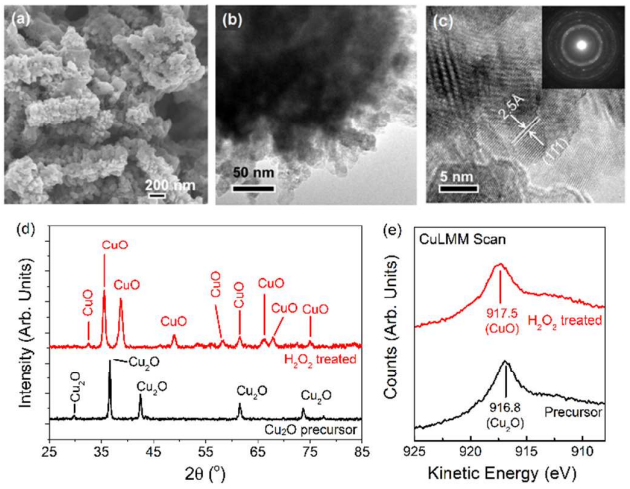


**Figure 1:** Scanning and transmission electron microscopy images of (a-c) $H_2O_2$-treated CuO nanostructures. (d) X-ray diffractograms and (e) Auger Cu LMM signals of $Cu_2O$ nanostructures before (black traces) and after $H_2O_2$ treatment (red traces). The selected area electron diffraction (SAED) ring patterns and d-spacing shown in (c) match that of CuO.

CuO particles on Cu surfaces.[31] Attempts to reproduce these CuO structures by heating the nanostructured $Cu_2O$ precursors at 400 °C in air gave only 200-300 nm sized CuO particles (supporting information section 2). This implies that chemical oxidation of $Cu_2O$ by $H_2O_2$ is unique in forming CuO nanostructures with the as-observed nanoscale features.

The oxygen evolution activities of the CuO nanostructures and the $Cu_2O$ precursor were assessed by linear sweep voltammetry (LSV) in 0.1 M KOH electrolyte. For comparison, measurements were also performed on commercially-available $Cu_2O$ particles and electrodeposited $Cu^0$ nanoparticulate films (supporting information sections 1.2.3 and 3). Among the Cu catalysts, $H_2O_2$-treated CuO nanostructures exhibited the best OER performance, with a relatively early OER onset potential of ~1.57 V (Figure 2a). At 1.75 V, a current density of >2.5 $mA/cm^2$ was recorded (Figure 2a). The untreated $Cu_2O$ precursors were comparatively less active, displaying approximately half of the CuO nanostructures' anodic current. Electrodeposited Cu nanoparticles did not display any clear OER activity, and only a weak current density of ~0.15 $mA/cm^2$ was recorded at 1.75 V.

Chronoamperometric measurements at 1.75 V over 1 hr were made to corroborate the as-observed electrochemical activities and to determine the stabilities of the catalysts (Fig 2b). Comparing catalysts held under a constant potential is also a more realistic way to assess operating performance during actual water electrolysis. The current density exhibited by the $H_2O_2$-treated CuO nanostructures remained highly stable at ~3.4 $mA/cm^2$ after 1 hour of OER (Fig 2b). Online mass spectrometry measurements during chronoamperometry confirmed that the gaseous product was $O_2$ (supporting information section 4).

In contrast, the catalytic activity of CuO obtained by heat treating the $Cu_2O$ precursor was relatively unstable and decreased by 75% to <1 $mA/cm^2$ after 30 minutes of OER

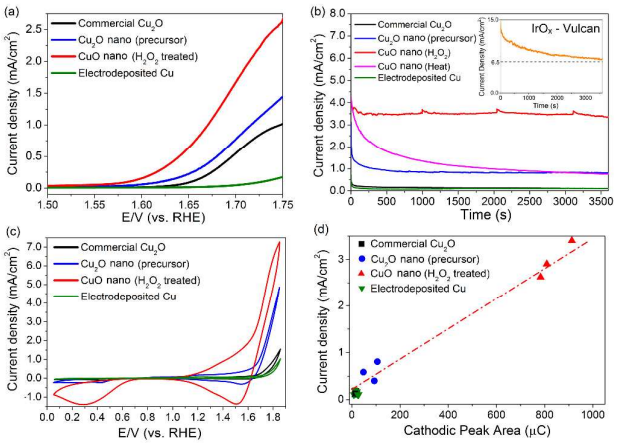


Figure 2: (a) Linear sweep voltammograms and (b) chronoamperograms (at 1.75 V) of copper samples. The chronoamperogram of 20% IrOx/Vulcan XC-72 catalyst is shown in the insert in (b). (c) Cyclic voltammograms of copper samples. (d) Correlation plot between cathodic peak areas vs. chronoamperometry current densities (measured at 2200 sec). A line was drawn in Fig 2d as a guide to the eye.

(Figure 2b). For further reference, we measured the benchmark 20% IrOx/Vulcan XC-72 catalyst under the same electrochemical conditions (Insert in Figure 2b). While its current density is initially ≥2× higher than the $H_2O_2$-treated CuO nanostructures, its performance deteriorate rather quickly. This phenomenon, which has been observed in previous OER studies utilising iridium, can be attributed to either carbon corrosion or the dissolution of $IrO_x$ to water-soluble $Ir^{VI}$.[5]

A conservative estimate of the turnover frequency (TOF) of $O_2$ evolution at 1.75 V (η = 520 mV) by the $H_2O_2$-treated CuO nanostructures is $2.4\times10^{-3}$ to $2.9\times10^{-3}$ $s^{-1}$ (assuming all Cu atoms are participating in the reaction, supporting information section 5). This value is 4 to 7× higher than that of as-grown $Cu_2O$ nanostructures ($4.3\times10^{-4}$ - $6.0\times10^{-4}$ $s^{-1}$), and 40 to 68× higher than electrodeposited Cu metal ($4.3\times10^{-5}$ - $6.0\times10^{-5}$ $s^{-1}$). This is also approximately two orders of magnitude higher than the values (~$10^{-5}$ $s^{-1}$) exhibited by Cu or $Cu_2O$ nanoparticles in earlier works.[17, 18] Furthermore, the TOF value of our CuO nanostructures compares favourably to the TOFs of other reported OER catalysts including $CaMn_2O_5$,[32] nano β-$MnO_2$,[33] $Co_3O_4$[34, 35] and cobalt phosphate.[36] Thus, a simple hydrothermal synthesis and subsequent oxidation process using $H_2O_2$ has produced CuO nanostructures that has an OER activity comparable or even higher than that of many other cobalt- and manganese- based compounds (using observed current densities and calculated TOFs at fixed overpotentials as figures of merit; Table S6).[17, 18, 32-36] This is highly significant since manganese and cobalt compounds are among the most promising substitutes for Ir and Ru oxides for electrochemical oxygen evolution.[37] We also found that metallic Cu discs oxidised by our $H_2O_2$ treatment yield improvements in their OER activities. This will facilitate the larger scale use of Cu-based OER catalysts (supporting information section 6).

The surface roughness of the Cu catalysts varied within a factor of three (supporting information section 7). Hence, the enhanced OER activity exhibited by the $H_2O_2$-treated CuO nanostructures cannot be totally attributed to differences in surface area. We hypothesised that its efficacy could have been underpinned by its unique chemical composition during OER. Cyclic voltammetry scans of the catalysts were thus performed in 0.1 M KOH electrolyte (Figure 2c) to investigate the cause. A significant cathodic peak at 1.5 - 1.6 V was found in the CV scans of the copper and copper oxide samples. Cathodic peaks observed at this potential regime have been attributed by Miller, El Haleem and other workers to the reduction of $Cu^{III}$ species.[21-23] Interestingly, we found that the amount of charges beneath the cathodic peak of each catalyst is proportional to their OER current density measured during chronoamperometry (Figure 2d). This correlation suggests that the OER activity of the Cu catalysts is closely related to the surface population of $Cu^{III}$. To rule out the possibility that the observed cathodic peak at 1.5 - 1.6 V was from the re-deposition of dissolved Cu ions, repeated LSV scans of the $H_2O_2$-treated CuO nanostructures were made over 2 hrs (supporting information section 8). The measured currents were found to be highly stable.

To elucidate the presence and role of catalytic active Cu species for OER, we turn to in-situ Raman spectroscopy. For these measurements, $Cu_2O$ precursors and $H_2O_2$-treated CuO nanostructures were grown on Cu disc substrates (supporting information section 9). The in-situ Raman spectra and chronoamperograms of the electrodes were then simultaneously measured in 0.1 M KOH electrolyte (Figure 3).

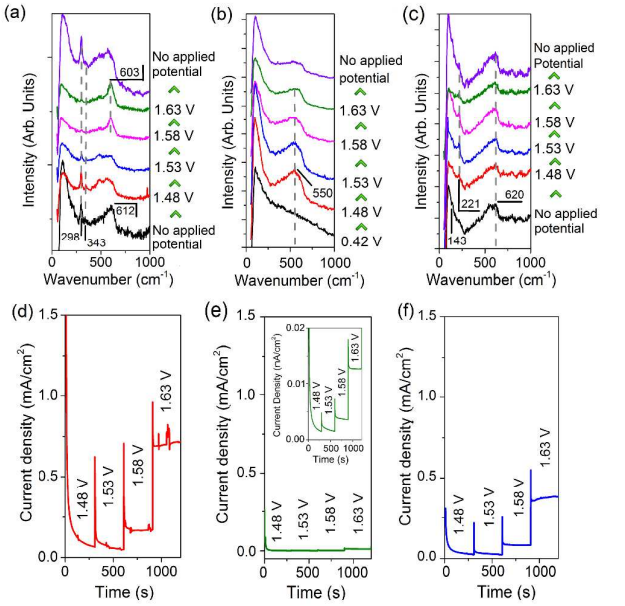


**Figure 3:** In-situ Raman spectra of (a) $H_2O_2$-treated CuO nanostructures, (b) Cu electrode, and (c) $Cu_2O$ precursor collected at different applied potentials. The corresponding chronoamperograms are presented below their Raman spectra in (d-f) respectively. The insert in (e) is a zoomed-in of the chronoamperogram of Cu.

The Raman spectra of $H_2O_2$-treated CuO nanostructures are presented in Figure 3a. Without applied potential, characteristic CuO bands at 298, 343 and 612 $cm^{-1}$ (broad) were observed.[38] Very interestingly, as the film was subjected to more anodic electrochemical potentials, a sharp peak at 603 $cm^{-1}$ appears at the expense of the CuO peaks. This feature dominated the spectrum at 1.63 V where OER occurs. However, it proved to be transient as it disappeared as soon as the applied potential was removed (with the restoration of the CuO peaks, Figure 3a). These observations demonstrate that the band at 603 $cm^{-1}$ originates from CuO species, and its generation and stabilisation is dependent on the applied potential.To the best of our knowledge, no Raman peak at 603 $cm^{-1}$ have been observed on copper or copper oxide surfaces with or without electrochemical bias. This peak also cannot be assigned to CuO, $Cu(OH)_2$, $Cu_2O$, or adventitious impurities (supporting information section 9).[38-42] Instead, consistent with thermodynamics and with cyclic voltammetry data that $Cu^{III}$ oxide is formed at oxygen evolving potentials, we ascribed the 603 $cm^{-1}$ band to the Cu-O stretching vibration of $Cu^{III}$ oxide.[22-24] This assignment is supported by the occurrence of a Raman peak at 603 $cm^{-1}$ belonging to the $Cu^{III}$ containing compound, $NaCuO_2$ (supporting information section 10). Furthermore, the $Cu^{III}$-O stretching vibration of the bis-($\mu$-oxo)-$Cu^{III}_2$ core of copper complexes is at ~608 $cm^{-1}$.[43]

In contrast, only a broad band centred at ~550 $cm^{-1}$ was observed in the Raman spectra of metallic Cu during OER (Figure 3b). This feature could be attributed to the formation of amorphous Cu oxides. No trace of CuO was detected even at 1.63 V. This is consistent with a previous report on anodisation of metallic Cu in basic electrolyte using stepped voltages to transpassive regions where no CuO could be formed.[44] On the $Cu_2O$ nanostructures, a broad band at 540-620 $cm^{-1}$ that could originate from a mixture of amorphous Cu oxides, $Cu_2O$ and $Cu^{III}$ oxide was recorded, alongside the $Cu_2O$ characteristic peak at 221 $cm^{-1}$ (Figure 3c).

The widely accepted reaction mechanism for OER on oxide surfaces consists of a sequence of four consecutive one-electron oxidations (Figure 4).[45, 46] The oxygen coupling step produces a –$OOH^*$ intermediate, which then dissociates to produce $O_2$. Based on this reaction scheme, it is possible that a higher oxidation state of $Cu^{III}$ could enhance the electrophilicity of the adsorbed O, and hence promote the formation of O-$OH^*$ via nucleophilic attack from an incoming $OH^-$. The $Cu^{III}$ are also likely to facilitate the deprotonation of –$OOH^*$, through electron withdrawing inductive effects, to give molecular $O_2$.[11] Our proposition is supported by previous studies which suggest that high valent metal cations such as $Fe^{VI}$ are the active sites for catalysing OER.[47] The presence of the intense and sharp Raman peak at 603 $cm^{-1}$ in the spectra of $H_2O_2$-treated CuO nanostructures demonstrate that the OER-active $Cu^{III}$ species is able to form and accumulate easily on it (Figure 3a). Metallic Cu, on the other hand, could not be oxidised directly to CuO by the application of a single anodic potential step.[44] Thus, $Cu^{III}$ species could not be generated readily on its surface at high potentials, leading to its weaker OER performance.

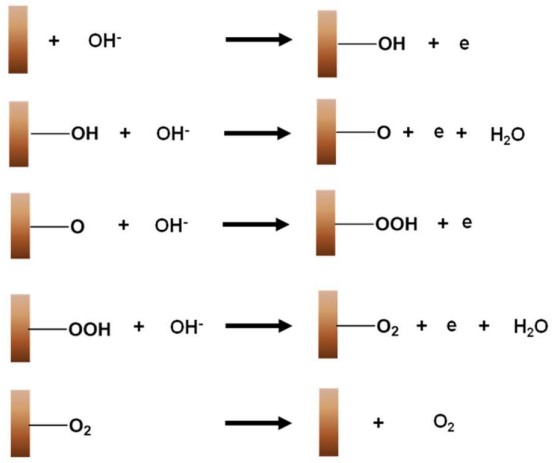


**Figure 4:** A schematic diagram illustrating the mechanism for the electrochemical oxygen evolution reaction on copper.

A previous OER study using Co, CoO and $Co_3O_4$ nanoparticles have shown that their overall activity is independent of their initial oxidation state.[28] This is because all three catalysts oxidise to a common species, believed to be $Co^{IV}$, as oxygen evolving potentials are reached. This work, however, demonstrates that the initial oxidation state of a Cu surface can significantly influence the type of catalytic species formed during OER, and hence its overall $O_2$ production. The use of $H_2O_2$ as oxidant serves to remove amorphous carbon formed during synthesis,[48] which can obscure active sites on the CuO nanostructures and inhibit their catalytic activities.[49] Another important contribution of this work is that expensive metallic dopants such as Rh or Au were not used to enhance the $O_2$-evolving activity of the CuO nanostructures.[11, 19] Finally, we do note that the performance of our CuO nanostructures still trails that of Ru and Ir oxides. One reason for this could be their relatively low conductivity, which could be addressed by dispersing them in a conductive carbon support or by further reducing their dimensions. Our timely discovery of the active oxidation states of copper during OER is a critical knowledge for other workers to consider when engineering Cu-based compounds with activities that could eventually match those of expensive state-of-the-art catalysts.

## Conclusions

In this work, we demonstrate that a simple hydrothermal synthesis and subsequent $H_2O_2$ oxidation treatment yields CuO nanostructures that exhibit sustainable and excellent OER activity. The OER activity of these $H_2O_2$-treated CuO nanostructures is enhanced such that they are 40-68× higher than that of electrodeposited Cu metal, and about half of 20% $IrO_x$/Vulcan XC-72 commercial OER catalyst. Another notable finding is that the $H_2O_2$-treated CuO is catalytically robust as demonstrated by its stable OER current during chronoamperometry. In-situ Raman spectroscopy of the Cu

catalysts during OER revealed the presence of a transient species that was more readily formed on the surface of $H_2O_2$-treated CuO nanostructures than $Cu_2O$ nanostructures or metallic Cu. This species, which we assigned to be $Cu^{III}$ oxide, are proposed as active sites for catalysing OER. The discovery of an OER active species on copper oxide surfaces is unprecedented. The knowledge gained in this work will help us to engineer and enhance the OER catalytic activity of Cu-based compounds, to a level that is competitive with other more established catalysts.

## Experimental Section

**Synthesis**

Nanostructured CuO powders were prepared by the $H_2O_2$ oxidation treatment of $Cu_2O$ nanostructured precursors. The latter were grown hydrothermally from an aqueous solution of $Cu^{II}$ acetate (≥98%, Sigma Aldrich), graphene oxide and *o*-anisidine (>99%, Sigma Aldrich) in a Teflon lined autoclave.[50] Oxidation treatment was performed by immersing 10 mg of the nanostructured $Cu_2O$ precursors in 1 ml $H_2O_2$ (30 vol%, Scharlau) for 1 hour at 60 °C. This was followed by 5 rinses with deionised water and drying overnight at 60 °C. This process was performed five times. $Cu_2O$ precursor films for spectroscopy analyses were grown directly onto polished 10 mm diameter copper discs (99.99+%, Goodfellow Cambridge Limited) during the hydrothermal process described above. CuO nanostructured film was obtained by immersing $Cu_2O$ precursor films in ~5 ml of $H_2O_2$ inside a Teflon lined autoclave.

**Preparation of catalyst ink**

Catalyst inks were prepared by mixing 2 mg of the as-synthesized catalyst, 0.1 ml iso-propanol (analytical reagent, Fisher), 0.4 ml of deionised $H_2O$ (≥18.2 MΩ·cm, Barnstead) and 60 µL of Nafion 117 solution (Sigma Aldrich). The suspensions were sonicated at 20 °C for 30 minutes to ensure even mixing. 5 µL of the catalyst ink was then drop-casted onto polished glassy carbon electrodes (3 mm diameter, CH Instruments). 17.9 µg of catalyst was typically loaded on each electrode. Catalyst inks of 20% Ir-Vulcan XC-72 (Premetek), and $Cu_2O$ (99.9%, Alfa Aesar) were similarly prepared.

**Electrochemical measurements**

The electrochemical measurements were performed in a glass H-cell with a 3-electrode configuration. A Ag/AgCl (saturated KCl gel) electrode (Pine Instruments) and a platinum wire were used respectively as reference and counter electrodes. The electrolyte is 0.1 M KOH solution (99.98%, Alfa Aesar). A Gamry Reference 600 potentiostat was used for controlling and measuring potentials / currents. No iR compensation was applied to the measurements because of the low net current and conductive electrolyte. Cyclic and linear sweep voltammetries were conducted at respective scan rates of 50 and 1 mV $s^{-1}$. All electrochemical measurements were conducted at 25 °C. All potentials cited in this work are with respect to the reversible hydrogen electrode (RHE). No trace of $Cl^-$ could be detected in the electrolyte before and after electrochemical measurements (using a $Cl^-$ ion selective electrode).

**Materials characterisation**

Powder X-ray diffraction was carried out using a Siemens 5005 (Cu Kα radiation with graphite monochromator) while film samples were scanned using Bruker Discover D8 GADDS with general area detector (microfocused Cu Kα radiation). Particle morphology was examined using a scanning electron microscope (JEOL-6701F, secondary electron mode, 5 kV, 10 mA) and transmission electron microscopy (TEM, JEOL JEM-3010). XPS and Auger spectroscopy analysis were carried out using a VG ESCA 220i-XL Imaging XPS. These measurements used the monochromatic Al Kα X-ray ($h\nu$ = 1486.6 eV) with photoelectron collection angle of 90° with respect to surface plane.

In-situ Raman spectra were collected using an epi-illumination Raman microscope (Horiba Jobin Yvon). The electrochemical cell, designed and constructed in-house, was based on a round Teflon dish.[51] A Hg/HgO in 0.1 M KOH (CH Instrument) and Pt wire were used as reference and counter electrodes respectively. The electrochemical potentials were applied by an Autolab PGSTAT potentiostat from 1.48 V to 1.63 V in 0.05 V increments. Each potential was held constant while the Raman spectrum (acquisition time: 10 seconds × 3 cycles) was acquired. A He-Ne laser (632.8 nm, CVI Melles Griot) was used as the excitation source.

## Acknowledgements

This work is primarily supported by a start-up grant (R-143-000-515-133) and an academic research fund (R-143-000-587-112) from the National University of Singapore. We also acknowledge financial support from the National Research Foundation and Economic Development Board (SPORE, COY-15-EWI-RCFSA/N197-1). SCH and DS acknowledge the support of Singapore National Research Foundation under CRP Award No. NRF-CRP-4-2008-03. ADH is grateful to a research fellowship from the Singapore-Peking Oxford Research Enterprise (R-706-000-100-414).

## References

1. Y. Surendranath, D. K. Bediako and D. G. Nocera, *Proc. Natl. Acad. Sci. U. S. A.*, 2012, **109**, 15617-15621.
2. H. Ma, C. Liu, J. Liao, Y. Su, X. Xue and W. Xing, *J. Mol. Catal. A: Chem.*, 2006, **247**, 7-13.
3. Y. Lee, J. Suntivich, K. J. May, E. E. Perry and Y. Shao-Horn, *J. Phys. Chem. Lett.*, 2012, **3**, 399-404.
4. L. D. Burke, O. J. Murphy, J. F. O'Neill and S. Venkatesan, *J. Chem. Soc., Faraday Trans. 1*, 1977, **73**, 1659-1671.
5. C. C. L. McCrory, S. Jung, J. C. Peters and T. F. Jaramillo, *J. Am. Chem. Soc.*, 2013, **135**, 16977-16987.
6. S. Roberts and G. Gunn, in *Critical Metals Handbook*, ed. G. Gunn, Wiley, West Sussex, UK, 2013, ch. 6.
7. W. M. Haynes, *CRC Handbook of Chemistry and Physics, 95th Edition*, Taylor & Francis, 2014.

8. Y. Sui, W. Fu, H. Yang, Y. Zeng, Y. Zhang, Q. Zhao, Y. Li, X. Zhou, Y. Leng, M. Li and G. Zou, *Cryst. Growth Des.*, 2009, **10**, 99-108.
9. M. J. Siegfried and K.-S. Choi, *J. Am. Chem. Soc.*, 2006, **128**, 10356-10357.
10. M. Csuros and C. Csuros, *Environmental Sampling and Analysis for Metals*, Taylor & Francis, 2002.
11. B. S. Yeo and A. T. Bell, *J. Am. Chem. Soc.*, 2011, **133**, 5587-5593.
12. L. Brossard and B. Marquis, *Int. J. Hydrogen Energy*, 1994, **19**, 231-237.
13. M. Biton, G. Salitra, D. Aurbach, P. Mishkov and D. Ilzycer, *J. Electrochem. Soc.*, 2006, **153**, B555-B565.
14. D. W. Shoesmith, S. Sunder, M. G. Bailey, G. J. Wallace and F. W. Stanchell, *J. Electroanal. Chem. Interfacial Electrochem.*, 1983, **143**, 153-165.
15. J. S. Halliday, *Trans. Faraday Soc.*, 1954, **50**, 171-178.
16. B. Marsan, N. Fradette and G. Beaudoin, *J. Electrochem. Soc.*, 1992, **139**, 1889-1896.
17. B. Kumar, S. Saha, M. Basu and A. K. Ganguli, *J. Mater. Chem. A*, 2013, **1**, 4728-4735.
18. B. Kumar, S. Saha, A. Ganguly and A. K. Ganguli, *RSC Adv.*, 2014, **4**, 12043-12049.
19. R. Hinogami, K. Toyoda, M. Aizawa, S. Yoshii, T. Kawasaki and H. Gyoten, *Electrochem. Commun.*, 2013, **35**, 142-145.
20. J. Wang, K. Wang, F.-B. Wang and X.-H. Xia, *Nat Commun*, 2014, **5**.
21. J. Ambrose, R. G. Barradas and D. W. Shoesmith, *J. Electroanal. Chem. Interfacial Electrochem.*, 1973, **47**, 47-64.
22. B. Miller, *J. Electrochem. Soc.*, 1969, **116**, 1675-1680.
23. S. M. Abd el Haleem and B. G. Ateya, *J. Electroanal. Chem. Interfacial Electrochem.*, 1981, **117**, 309-319.
24. A. M. S. El Din and F. M. A. El Wahab, *Electrochim. Acta*, 1964, **9**, 113-121.
25. M. Pourbaix, in *Lectures on Electrochemical Corrosion*, ed. R. W. Staehle, Springer US, New York, 1st edn., 1973, DOI: 10.1007/978-1-4684-1806-4_7, ch. 7, pp. 297-314.
26. D. T. Schwartz and R. H. Muller, *Surf. Sci.*, 1991, **248**, 349-358.
27. M. E. G. Lyons and M. P. Brandon, *Int. J. Electrochem. Sci.*, 2008, **3**, 1425-1462.
28. N. H. Chou, P. N. Ross, A. T. Bell and T. D. Tilley, *ChemSusChem*, 2011, **4**, 1566-1569.
29. J. P. Lorimer, T. J. Mason, M. Plattes and D. J. Walton, *J. Electroanal. Chem.*, 2004, **568**, 379-390.
30. J. F. Moulder and J. Chastain, *Handbook of X-ray Photoelectron Spectroscopy: A Reference Book of Standard Spectra for Identification and Interpretation of XPS Data*, Physical Electronics Division, Perkin-Elmer Corporation, 1992.
31. J.-C. Chen and W.-T. Tsai, *Mater. Chem. Phys.*, 2004, **87**, 387-393.
32. J. Kim, X. Yin, K.-C. Tsao, S. Fang and H. Yang, *J. Am. Chem. Soc.*, 2014, **136**, 14646-14649.
33. M. Fekete, R. K. Hocking, S. L. Y. Chang, C. Italiano, A. F. Patti, F. Arena and L. Spiccia, *Energy Environ. Sci.*, 2013, **6**, 2222-2232.
34. C. Iwakura, A. Honji and H. Tamura, *Electrochim. Acta*, 1981, **26**, 1319-1326.
35. P. Rasiyah and A. C. C. Tseung, *J. Electrochem. Soc.*, 1983, **130**, 365-368.
36. M. W. Kanan and D. G. Nocera, *Science*, 2008, **321**, 1072-1075.
37. M. W. Kanan, Y. Surendranath and D. G. Nocera, *Chem. Soc. Rev.*, 2009, **38**, 109-114.
38. L. Debbichi, M. C. Marco de Lucas, J. F. Pierson and P. Krüger, *J. Phys. Chem. C*, 2012, **116**, 10232-10237.
39. D. Reyter, M. Odziemkowski, D. Bélanger and L. Roué, *J. Electrochem. Soc.*, 2007, **154**, K36-K44.
40. G. Niaura, *Electrochim. Acta*, 2000, **45**, 3507-3519.
41. S. T. Mayer and R. H. Muller, *J. Electrochem. Soc.*, 1992, **139**, 426-434.
42. H. Y. H. Chan, C. G. Takoudis and M. J. Weaver, *J. Phys. Chem. B*, 1998, **103**, 357-365.
43. M. J. Henson, M. A. Vance, C. X. Zhang, H.-C. Liang, K. D. Karlin and E. I. Solomon, *J. Am. Chem. Soc.*, 2003, **125**, 5186-5192.
44. N. Fredj and T. D. Burleigh, *J. Electrochem. Soc.*, 2011, **158**, C104-C110.
45. I. C. Man, H.-Y. Su, F. Calle-Vallejo, H. A. Hansen, J. I. Martínez, N. G. Inoglu, J. Kitchin, T. F. Jaramillo, J. K. Nørskov and J. Rossmeisl, *ChemCatChem*, 2011, **3**, 1159-1165.
46. J. Rossmeisl, Z. W. Qu, H. Zhu, G. J. Kroes and J. K. Nørskov, *J. Electroanal. Chem.*, 2007, **607**, 83-89.
47. M. E. G. Lyons and M. P. Brandon, *J. Electroanal. Chem.*, 2010, **641**, 119-130.
48. Y. Feng, G. Zhou, G. Wang, M. Qu and Z. Yu, *Chem. Phys. Lett.*, 2003, **375**, 645-648.
49. Y. C. Kimmel, D. V. Esposito, R. W. Birkmire and J. G. Chen, *Int. J. Hydrogen Energy*, 2012, **37**, 3019-3024.
50. S. Deng, V. Tjoa, H. M. Fan, H. R. Tan, D. C. Sayle, M. Olivo, S. Mhaisalkar, J. Wei and C. H. Sow, *J. Am. Chem. Soc.*, 2012, **134**, 4905-4917.
51. B. S. Yeo and A. T. Bell, *J. Phys. Chem. C*, 2012, **116**, 8394-8400.

## Table of Content Entry

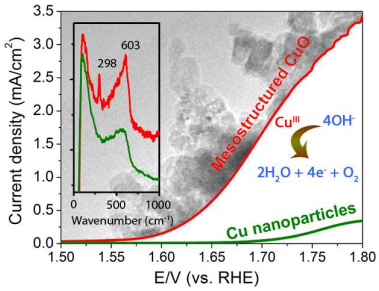


Thorough electrochemical and *in-situ* Raman spectroscopy provide a never-before reported evidence of $Cu^{III}$ involvement during OER on mesostructured Cu(II) oxides.